Dissociating H 2 +(2∑g +, JM =00) Ion as an Exploding Quantum Bubble

ARTICLE *in* THE JOURNAL OF PHYSICAL CHEMISTRY A · MARCH 2015

Impact Factor: 2.69 · DOI: 10.1021/acs.jpca.5b00907 · Source: PubMed

1 AUTHOR:

Jhon Fredy Perez-Torres

Freie Universität Berlin

36 PUBLICATIONS **457** CITATIONS

SEE PROFILE

THE JOURNAL OF PHYSICAL CHEMISTRY A

Article

pubs.acs.org/JPCA

Dissociating $H_2^+(^2\Sigma_g^+,JM{=}00)$ Ion as an Exploding Quantum Bubble

Jhon Fredy Pérez-Torres*

Institut für Chemie und Biochemie, Freie Universität Berlin, Takustraße 3, 14195 Berlin, Germany

ABSTRACT: The nuclear and electronic probability and flux densities for a vibrating and dissociating H_2^+ molecular ion in the electronic and rotational ground state (corresponding to the quantum numbers $^2\Sigma_g^+,JM = 00$) are calculated. As a consequence of the isotropy of the scenario, the vibrating H_2^+ appears as a pulsating quantum bubble, while the dissociating H_2^+ appears as an exploding quantum bubble. The dissociating part is represented by a discretization of the continuum through use of $\mathcal{L}^2$ integrable *B*-spline basis set. It is shown that the vibrating part (the pulsating quantum bubble) interferes with the dissociating part (the exploding quantum bubble) and that the interference is much more noticeable in the probability density than in the flux density.

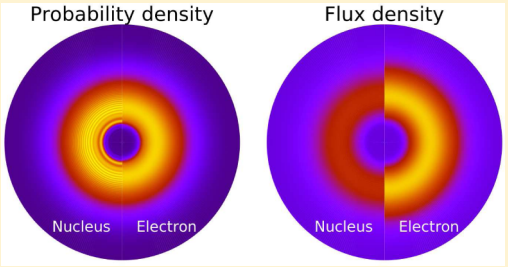

1. INTRODUCTION

The spatiotemporal description of a molecular system is entirely contained in the wave function, as established by Schrödinger.[1] However, this important quantity cannot be measured. Nevertheless, Schrödinger defined two space- and time-dependent quantities, which, in principle, are observables. They are the probability density distribution and the flux density distribution, which are related to each other through the continuity equation. For a diatomic molecule, the nuclear probability density distribution and the nuclear flux density distribution, or simply the nuclear probability density and the nuclear flux density, can be expressed in terms of the internuclear vector, $\mathbf{R}$, at time, t, that is, $\rho_n(\mathbf{R},t)$ and $\mathbf{j}_n(\mathbf{R},t)$, respectively. If the system is prepared in a stationary state; then, $\rho_n(\mathbf{R},t)$ becomes time-independent and $\mathbf{j}_n(\mathbf{R},t)$ just vanishes.

During the last 15 years the development of pump−probe spectroscopy has allowed the construction of $\rho_n(|\mathbf{R}|,t)$, for instance, for the Na_2 molecule vibrating in the $2^1\Pi_g$ electronic state,[2] and for the D_2^+ molecular ion vibrating in the $^2\Sigma_g^+$ electronic state.[3] Knowledge of $\rho_n(|\mathbf{R}|,t)$ is important because it provides detailed information about molecular vibrations, for instance, dephasing and revival of the nuclear wave packets.[3−5] Moreover, the nuclear flux density $\mathbf{j}_n(|\mathbf{R}|,t)$ has been also constructed from $\rho_n(|\mathbf{R}|,t)$ by means of the continuity equation with appropriate boundary conditions. This has revealed new quantum effects and is a key observable for understanding the nuclear dynamics.[6] Pump−probe experiments may lead to the photoionization of the molecular system. At the same time, the photoionization produces vibrating and dissociating molecular ions. For example, in the ionization of H_2 with photons of energy around 25 eV, 98% goes to vibration, while the remaining 2% leads to dissociation.[7]

Both vibration and dissociation should be taken into account in a proper description of not only $\rho_n(\mathbf{R},t)$ and $\mathbf{j}_n(\mathbf{R},t)$ but also $\rho_e(\mathbf{r},t)$ and $\mathbf{j}_e(\mathbf{r},t)$ (the electronic probability density and the electronic flux density). The calculation of the electronic flux density associated with vibration and also dissociation in the electronic ground state of a molecular system is a challenge[8] because the customary practice of describing the state in the Born−Oppenheimer approximation gives a *real* electronic wave function, for which the electronic flux density vanishes.[1] This failure of the Born−Oppenheimer approximation has been carefully studied in the aligned vibrating $H_2^+(^2\Sigma_g^+)$ system.[9−13] Calculation of the electronic probability and flux densities are important because together with the nuclear densities they furnish a detailed description of the correlated electronic-nuclear dynamics. For example, from the analysis of the nuclear and electronic flux densities, one realizes that the nuclear wave packet needs slightly more time (1.4 fs) to change direction than the electronic one (1 fs) in the aligned vibrating H_2^+ molecular ion.[13]

We note that if the system is isotropic, we can make use of the radial continuity equation to access to the electronic flux density. Such is the case of $H_2^+(^2\Sigma_g^+,JM = 00)$ vibrating in the electronic and rotational ground state (pulsating quantum bubble).[14] Here we calculate the four quantum observables: $\rho_n(\mathbf{R},t)$, $\mathbf{j}_n(\mathbf{R},t)$, $\rho_e(\mathbf{r},t)$, and $\mathbf{j}_e(\mathbf{r},t)$ not only for a vibrating but also for a dissociating isotropic H_2^+ molecular ion, employing the formalism developed previously.[14] We assume that the Born−Oppenheimer approximation is adequate and that the system remains in the $^2\Sigma_g^+$ electronic ground state. The electronic part of the wave function is calculated by the linear combination of atomic orbitals (LCAO) Hartree−Fock technique, which properly describes the asymptotic limit $H(1s) + H^+$. Special attention is paid to the dissociating part. The method discretizes the continuum (i.e., the states representing the continuum are box normalized) through use of the $\mathcal{L}^2$ integrable *B*-spline basis set,[15,16] which is well-known to be suited to the challenging numerical task of computing accurate nuclear wave functions for large internuclear distances.[17]

Received: January 28, 2015
Revised: March 9, 2015
Published: March 9, 2015

DOI: 10.1021/acs.jpca.5b00907
J. Phys. Chem. A 2015, 119, 2895−2901

2. THEORY AND COMPUTATIONS

In this section we extend the quantum theory for electronic density and flux density of an isotropic vibrating H_2^+ molecular ion[14] to the case of an isotropic vibrating and dissociating H_2^+. Toward this goal our starting point is the same as the previous one;[14] that is, as a good approximation, we make the Born−Oppenheimer factorization for the molecular wave function

$$\Phi_{\mathrm{mol}}(\mathbf{r}, \mathbf{R}, t) = \psi_e(\mathbf{r}; R) \times \Psi_{\mathrm{nuc}}(\mathbf{R}, t) \tag{1}$$

where the electronic wave function $\psi_e(\mathbf{r};R)$ is the solution of the time-independent clamped-nuclei Schrödinger equation in the molecular frame

$$\left[-\frac{\hbar^2}{2m_e}\nabla_{\mathbf{r}}^2 - \frac{e^2}{4\pi\varepsilon_0 r_a} - \frac{e^2}{4\pi\varepsilon_0 r_b}\right]\psi_e(\mathbf{r}; R) = V(R)\psi_e(\mathbf{r}; R) \tag{2}$$

with $r_a = |\mathbf{r} - \mathbf{R}_a|$, $r_b = |\mathbf{r} - \mathbf{R}_b|$, $\mathbf{R} = \mathbf{R}_a - \mathbf{R}_b$, and $R = |\mathbf{R}|$, and the nuclear wave function $\Psi_{\mathrm{nuc}}(\mathbf{R},t)$ is the solution of the time-dependent Schrödinger equation

$$\left[-\frac{\hbar^2}{2\mu_n}\nabla_{\mathbf{R}} + V(R)\right]\Psi_{\mathrm{nuc}}(\mathbf{R}, t) = i\hbar\frac{\partial}{\partial t}\Psi_{\mathrm{nuc}}(\mathbf{R}, t) \tag{3}$$

2.1. Nuclear Motion. The nuclear wave function in the rotational ground state reads

$$\Psi_{\mathrm{nuc},JM=00}(\mathbf{R}, t) = \frac{\Psi_n(R, t)}{R}Y_{JM=00}(\Theta, \Phi) \tag{4}$$

with the spherical harmonic $Y_{JM=00}(\Theta,\Phi) = (4\pi)^{-1/2}$. Thus, the isotropic nuclear probability density is

$$\rho_n(\mathbf{R}, t) = \frac{1}{4\pi R^2}\Psi_n^*(R, t)\Psi_n(R, t) \tag{5}$$

and the isotropic nuclear flux density is

$$\mathbf{j}_n(\mathbf{R}, t) = \frac{1}{4\pi R^2}\Re\left[\Psi_n^*(R, t)\frac{\hat{P}_{\mathrm{R}}}{\mu_n}\Psi_n(R, t)\right]\mathbf{e}_{\mathrm{R}} \tag{6}$$

where $\hat{P}_{\mathrm{R}} = -i\hbar\partial/\partial R$ is the radial momentum operator. Formally, the radial wave function $\Psi_n(R,t)$ can be split into the following two terms

$$\Psi_n(R, t) = \Psi_{n,\mathrm{vib}}(R, t) + \Psi_{n,\mathrm{dis}}(R, t) \tag{7}$$

where $\Psi_{n,\mathrm{vib}}(R,t)$ and $\Psi_{n,\mathrm{dis}}(R,t)$ represent the vibration and the dissociation, respectively. Substitution of eq 7 into eq 6 leads to

$$\begin{aligned}\mathbf{j}_n(\mathbf{R}, t) = \frac{1}{4\pi R^2}\Re[&\Psi_{n,\mathrm{vib}}^*(R, t)\frac{\hat{P}_{\mathrm{R}}}{\mu_n}\Psi_{n,\mathrm{vib}}(R, t) \\ &+ \Psi_{n,\mathrm{dis}}^*(R, t)\frac{\hat{P}_{\mathrm{R}}}{\mu_n}\Psi_{n,\mathrm{dis}}(R, t) + \Psi_{n,\mathrm{vib}}^*(R, t) \\ &\times \frac{\hat{P}_{\mathrm{R}}}{\mu_n}\Psi_{n,\mathrm{dis}}(R, t) + \Psi_{n,\mathrm{dis}}^*(R, t)\frac{\hat{P}_{\mathrm{R}}}{\mu_n}\Psi_{n,\mathrm{vib}}(R, t)]\mathbf{e}_{\mathrm{R}} \\ = \mathbf{j}_{n,\mathrm{vib}}(\mathbf{R}, t) &+ \mathbf{j}_{n,\mathrm{dis}}(\mathbf{R}, t) + \Delta\mathbf{j}_{n,\mathrm{int}}(\mathbf{R}, t)\end{aligned} \tag{8}$$

where the vibrational, dissociative, and interfering nuclear flux densities are defined as

$$\mathbf{j}_{n,\mathrm{vib}}(\mathbf{R}, t) = \frac{1}{4\pi R^2}\Re\left[\Psi_{n,\mathrm{vib}}^*(R, t)\frac{\hat{P}_{\mathrm{R}}}{\mu_n}\Psi_{n,\mathrm{vib}}(R, t)\right]\mathbf{e}_{\mathrm{R}} \tag{9}$$

$$\mathbf{j}_{n,\mathrm{dis}}(\mathbf{R}, t) = \frac{1}{4\pi R^2}\Re\left[\Psi_{n,\mathrm{dis}}^*(R, t)\frac{\hat{P}_{\mathrm{R}}}{\mu_n}\Psi_{n,\mathrm{dis}}(R, t)\right]\mathbf{e}_{\mathrm{R}} \tag{10}$$

$$\begin{aligned}\Delta\mathbf{j}_{n,\mathrm{int}}(\mathbf{R}, t) = &\frac{1}{4\pi R^2}\Re\left[\Psi_{n,\mathrm{vib}}^*(R, t)\frac{\hat{P}_{\mathrm{R}}}{\mu_n}\Psi_{n,\mathrm{dis}}(R, t)\right]\mathbf{e}_{\mathrm{R}} \\ &+ \frac{1}{4\pi R^2}\Re\left[\Psi_{n,\mathrm{dis}}^*(R, t)\frac{\hat{P}_{\mathrm{R}}}{\mu_n}\Psi_{n,\mathrm{vib}}(R, t)\right]\mathbf{e}_{\mathrm{R}}\end{aligned} \tag{11}$$

In a similar manner, the nuclear probability density $\rho_n(\mathbf{R},t)$ can be partitioned as follows

$$\rho_n(\mathbf{R}, t) = \rho_{n,\mathrm{vib}}(\mathbf{R}, t) + \rho_{n,\mathrm{dis}}(\mathbf{R}, t) + \Delta\rho_{n,\mathrm{int}}(\mathbf{R}, t) \tag{12}$$

with

$$\rho_{n,\mathrm{vib}}(\mathbf{R}, t) = \frac{1}{4\pi R^2}\Psi_{n,\mathrm{vib}}^*(R, t)\Psi_{n,\mathrm{vib}}(R, t) \tag{13}$$

$$\rho_{n,\mathrm{dis}}(\mathbf{R}, t) = \frac{1}{4\pi R^2}\Psi_{n,\mathrm{dis}}^*(R, t)\Psi_{n,\mathrm{dis}}(R, t) \tag{14}$$

$$\begin{aligned}\Delta\rho_{n,\mathrm{int}}(\mathbf{R}, t) = &\frac{1}{4\pi R^2}\Psi_{n,\mathrm{vib}}^*(R, t)\Psi_{n,\mathrm{dis}}(R, t) + \frac{1}{4\pi R^2} \\ &\Psi_{n,\mathrm{dis}}^*(R, t)\Psi_{n,\mathrm{vib}}(R, t)\end{aligned} \tag{15}$$

Notice that the vibrating and dissociating parts of $\Psi_n(R,t)$ are not coupled (see eq 7), this leads to the interfering terms $\Delta\mathbf{j}_{n,\mathrm{int}}(\mathbf{R},t)$ and $\Delta\rho_{n,\mathrm{int}}(\mathbf{R},t)$. Both components of the radial wave function, $\Psi_{n,\mathrm{vib}}(R,t)$ and $\Psi_{n,\mathrm{dis}}(R,t)$, can be expanded in terms of the eigenfunctions of the nuclear Hamiltonian, $\hat{H}_{\mathrm{nuc}}$. Thus, we have

$$\Psi_{n,\mathrm{vib}}(R, t) = \sum_{\nu=0}^{K} c_\nu\xi_\nu(R)\mathrm{e}^{-\mathrm{i}E_\nu t/\hbar} \tag{16}$$

$$\Psi_{n,\mathrm{dis}}(R, t) = \sum_{\nu=K+1}^{N} c_\nu\xi_\nu(R)\mathrm{e}^{-iE_\nu t/\hbar} \tag{17}$$

where $N_{\mathrm{b}} = K + 1$ is the number of bound states (states with energy E_ν below the dissociation threshold) and $\xi_\nu(R)$ are solutions of the time-independent Schrödinger equation

$$\hat{H}_{\mathrm{nuc}}\xi_\nu(R) = \left[-\frac{\hbar^2}{2\mu_n}\frac{d^2}{dR^2} + V(R)\right]\xi_\nu(R) = E_\nu\xi_\nu(R) \tag{18}$$

Equation 18 is solved by expanding the eigenfunctions $\xi_\nu(R)$ in a $\mathcal{L}^2$ integrable B-spline basis set.[16] (See section 2.3.) This procedure yields a discrete spectrum (box-normalized eigenfunctions). The continuum is represented by the states lying above the dissociation threshold.[15] The expansion coefficients, c_ν, of the time-dependent nuclear wave functions are determined by the initial conditions. Here a Franck−Condon process is assumed for the ionization of the $H_2(^1\Sigma_g^+,\nu JM = 000)$ together with the propensity rule $\Delta J = 0$ observed by Åsbrink.[18] Thus, the expansion coefficients reduce to the projection of the nuclear wave function of the vibrational ground state of $H_2(^1\Sigma_g^+,\nu = 0)$ onto the vibrational wave functions of the $H_2^+(^2\Sigma_g^+,\nu)$

$$c_\nu = \int_0^\infty \Psi_{\mathrm{H}_2(^1\Sigma_g^+,\nu=0)}(R)\xi_\nu(R)\,\mathrm{d}R \tag{19}$$

DOI: 10.1021/acs.jpca.5b00907
J. Phys. Chem. A 2015, 119, 2895−2901

where $\Psi_{H_2(^1\Sigma_g^+,\nu=0)}(R)$ is the nuclear wave function of the vibrational ground state of H_2. Details of the calculation of $\Psi_{H_2(^1\Sigma_g^+,\nu=0)}(R)$ and the corresponding potential energy curve $V_{H_2(^1\Sigma_g^+)}(R)$ can be found in ref 14.

2.2. Electronic Motion. Expressions for the isotropic electronic probability density and flux densities start from the results of ref 14, where a detailed formulation is made. The isotropic time-dependent electronic probability density reads

$$\rho_e(r, t) = \int_0^\infty \mathrm{d}R\, R^2 \rho_n(R, t)\rho_e(r; R) \tag{20}$$

where

$$\rho_e(r; R) = \int_0^\pi \mathrm{d}\theta\, \sin\theta \int_0^{2\pi} \mathrm{d}\phi |\psi_e(r, \theta, \phi; R)|^2 \tag{21}$$

The partitioning of the nuclear probability density (see eq 12) leads to

$$\rho_{e,\mathrm{vib}}(r, t) = \int_0^\infty \mathrm{d}R\, R^2 \rho_{n,\mathrm{vib}}(R, t)\rho_e(r; R) \tag{22}$$

$$\rho_{e,\mathrm{dis}}(r, t) = \int_0^\infty \mathrm{d}R\, R^2 \rho_{n,\mathrm{dis}}(R, t)\rho_e(r; R) \tag{23}$$

$$\Delta\rho_{e,\mathrm{int}}(r, t) = \int_0^\infty \mathrm{d}R\, R^2 \Delta\rho_{n,\mathrm{int}}(R, t)\rho_e(r; R) \tag{24}$$

with

$$\rho_e(r, t) = \rho_{e,\mathrm{vib}}(r, t) + \rho_{e,\mathrm{dis}}(r, t) + \Delta\rho_{e,\mathrm{int}}(r, t) \tag{25}$$

The radial integration of the continuity equation for the electron leads to[14]

$$\mathbf{j}_e(r, t) = -\frac{1}{r^2}\int_0^r \mathrm{d}r' r'^2 \frac{\partial}{\partial t}\rho_e(r', t)\mathbf{e}_r \tag{26}$$

Thus, inserting eq 25 into eq 26 yields

$$\mathbf{j}_e(r, t) = \mathbf{j}_{e,\mathrm{vib}}(r, t) + \mathbf{j}_{e,\mathrm{dis}}(r, t) + \Delta\mathbf{j}_{e,\mathrm{int}}(r, t) \tag{27}$$

with

$$\mathbf{j}_{e,\mathrm{vib}}(r, t) = -\frac{1}{r^2}\int_0^r \mathrm{d}r' r'^2 \frac{\partial}{\partial t}\rho_{e,\mathrm{vib}}(r', t)\mathbf{e}_r \tag{28}$$

$$\mathbf{j}_{e,\mathrm{dis}}(r, t) = -\frac{1}{r^2}\int_0^r \mathrm{d}r' r'^2 \frac{\partial}{\partial t}\rho_{e,\mathrm{dis}}(r', t)\mathbf{e}_r \tag{29}$$

$$\Delta\mathbf{j}_{e,\mathrm{int}}(r, t) = -\frac{1}{r^2}\int_0^r \mathrm{d}r' r'^2 \frac{\partial}{\partial t}\Delta\rho_{e,\mathrm{int}}(r', t)\mathbf{e}_r \tag{30}$$

The expressions 28−30 invoke the boundary condition

$$\lim_{r\to\infty} r^2 \mathbf{j}_e(r, t) = 0 \tag{31}$$

2.3. Computational Details. The MOLPRO software[19] was employed to compute the electronic wave function $\psi_e(\mathbf{r};R)$ and potential energy curve $V(R)$ of the ground state by the LCAO Hartree−Fock technique over the range $0.7a_0 < R < 100.0a_0$ on an equidistant radial grid with $\Delta R = 0.1a_0$. The wave function is represented in the aug-cc-pVTZ atomic basis set. The aug-cc-pVTZ basis gives a potential energy of $V(R = 100.0a_0) = -0.4998E_h$, which is taken as the dissociation limit E_H. The ORBKIT software[20] was used to calculate $|\psi_e(r,\theta,\phi = 0;R)|^2$ on two regular radial grids: $0.001 < r < 0.09$, with $\Delta r = 0.001$ and $0.1 < r < 60.0$ with $\Delta r = 0.1$, together with the regular angular grid $0 < \theta < \pi/2$ with $\Delta\theta = \pi/400$. All of the integration was done by the Gauss-Legendre quadrature algorithm. The vibrational wave functions were expanded in a basis of B-spline functions, that is, $\xi_\nu(R) = \sum_\mu b_{\mu\nu} B_\mu(R)$. (See, for instance, ref 16 and references therein.) The expansion coefficients $b_{\mu\nu}$ were determined by solving the corresponding secular equation. One thousand eight hundred (1800) B-spline functions of order 8 linearly distributed within a box of length $R_{max} = 100.0a_0$ are employed. This calculation yields 20 bound states. A total of eight hundred states were included in the expansion of $\Psi_n(R,t)$, the 20 bound states to represent the vibration and 780 above-threshold states to represent the dissociation. This gives states with energy up to $-0.1533E_h$; that is, in the dissociation process, protons with energy up to $E_{H^+} = (-0.1533+E_H) \times 27.21/2 = 4.7$ eV can be released. The expansion is sufficient to cover the range of the kinetic-energy release spectrum for the dissociative photoionization of H_2 with photons of 20 eV, where the fastest protons produced have an energy of 1.25 eV.[7] The norm of the nuclear wave function is $\int_0^\infty |\Psi_n(R,t)|^2\, \mathrm{d}R = 1.0000$, while the populations of the vibrational and continuum states are $\int_0^\infty |\Psi_{n,\mathrm{vib}}(R,t)|^2\, \mathrm{d}R = 0.9860$ and $\int_0^\infty |\Psi_{n,\mathrm{dis}}(R,t)|^2\, \mathrm{d}R = 0.0140$, respectively. Figure 1 illustrates the ionization process and the initial conditions.

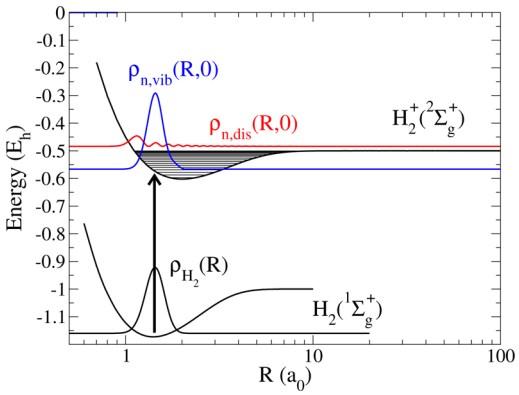

Figure 1. Model scenario for the preparation of the initial state of the vibrating and dissociating $H_2^+(^2\Sigma_g^+,JM = 00)$ by single-photon ionization of the precursor molecule $H_2(^1\Sigma_g^+,\nu JM = 000)$. The upper part of the Figure shows the nuclear vibrating density $\rho_{n,\mathrm{vib}}(R,t = 0)$ (embedded in its potential curve $V(R)$ with the corresponding vibrational levels indicated by horizontal lines) and the nuclear dissociating density $\rho_{n,\mathrm{dis}}(R,t = 0)$ of the $H_2^+(^2\Sigma_g^+,JM = 00)$. The vertical arrow symbolizes the Franck−Condon-type photoionization of $H_2(^1\Sigma_g^+,\nu JM = 000)$. The base lines of the densities correspond to their mean energies.

3. RESULTS AND DISCUSSION

Throughout this section we present all observables as functions of $\mathbf{r}$, the position vector (the point of observation) with respect to the nuclear center of mass (NCM). Thus, $\rho_n(\mathbf{r},t)$ and $\mathbf{j}_n(\mathbf{r},t)$ represent, respectively, the distribution of the probability density and flux density of either nucleus "a" or nucleus "b" with respect to the NCM. The new $\rho_n(\mathbf{r},t)$ and $\mathbf{j}_n(\mathbf{r},t)$ are related to $\rho_n(\mathbf{R},t)$ and $\mathbf{j}_n(\mathbf{R},t)$ through the following transformations[14]

$$8\rho_n(\mathbf{R} = 2\mathbf{r}, t) \rightarrow \rho_n(\mathbf{r}, t) \tag{32}$$

$$4j_n(\mathbf{R} = 2\mathbf{r}, t) \rightarrow j_n(\mathbf{r}, t) \tag{33}$$

DOI: 10.1021/acs.jpca.5b00907
J. Phys. Chem. A 2015, 119, 2895−2901

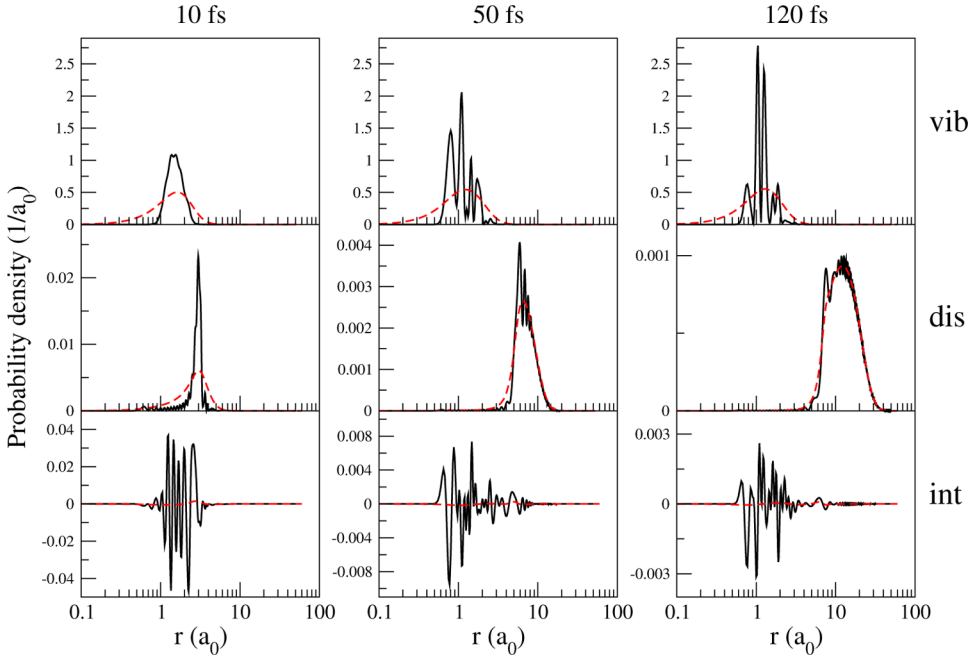

Figure 2. Snapshots of the radial part of the probability densities ($4\pi r^2\rho(r,t)$) at 10, 50, and 120 fs. r denotes the distance from the nuclear center of mass. Black solid lines: nuclear density; red dashed lines: electronic density. From top to the bottom: vibrating, dissociating, and interfering parts.

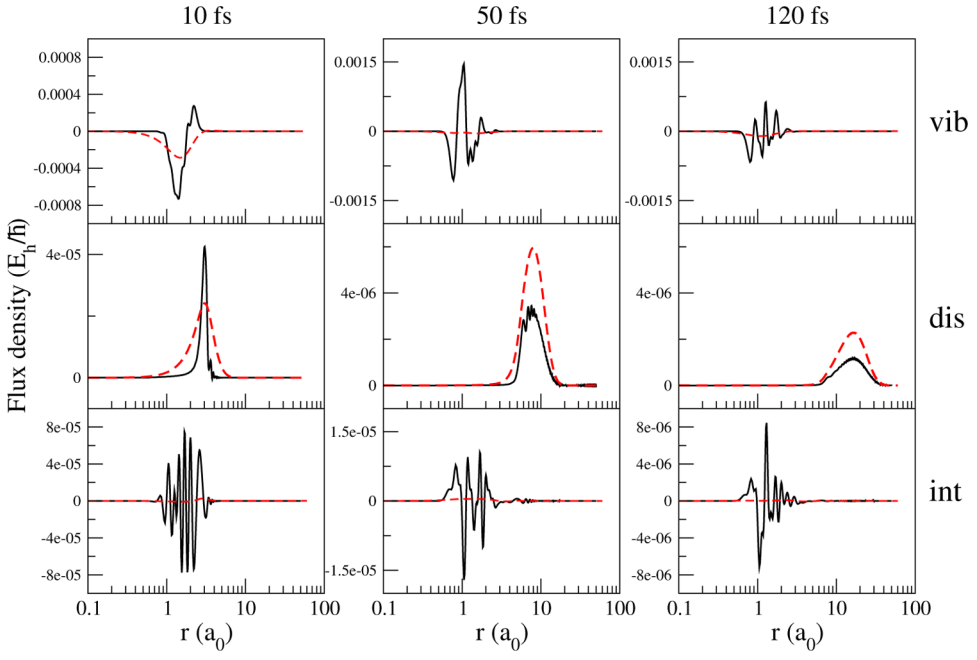

Figure 3. Snapshots of the radial part of the flux densities ($4\pi r^2 j(r,t)$) at 10, 50, and 120 fs. r denotes the distance from the nuclear center of mass. Black solid lines: nuclear flux; red dashed lines: electronic flux. From top to the bottom: vibrating, dissociating, and interfering parts.

The above switch facilitates the comparison of the electronic observables with the nuclear ones; after all, the electron is expected to travel with the two nuclei.

We consider first the gross features of the concerted nuclear and electronic probability and probability flux densities. Figure 2 displays the probability densities (the vibrating, dissociating, and interfering components) of the electron and the nuclei. Three different snapshots are displayed for times 10, 50, and 120 fs. The populations of the vibrational and continuum states are 0.9860 and 0.0140, respectively; that is, the probability of dissociation is about two orders of magnitude smaller than that of vibration. This can be clearly seen at 10 fs. As expected, the electronic probability density is, in general, distributed around the nuclear probability density. For the vibration, the electronic probability distribution is more diffuse compared with the nuclear distribution, corresponding to the chemical bond. Notice that the shape of the electronic probability distribution barely depends on time while the nuclear probability distribution starts with a Gaussian-type distribution at 10 fs (when the nuclear wave packet reaches the outer turning point) and becomes more complex with several maxima and minima (dephasing of the nuclear wave packet) after several round trips over the potential

DOI: 10.1021/acs.jpca.5b00907
J. Phys. Chem. A 2015, 119, 2895−2901

energy curve. (See the plots at 50 and 120 fs in Figure 2.) This can be understood as follows: Once $\Psi_{n,\mathrm{vib}}(\mathbf{R},t)$ reaches a classical turning point, the "head" of the nuclear wave packet switches direction being found with its "tail" causing the interferences exhibited by $\rho_{n,\mathrm{vib}}(r,t)$. For the dissociation, however, the electronic probability distribution is rather similar to the nuclear probability distribution (see the plots at 50 and 120 fs), thus corresponding already to two protons traveling in opposite directions, each with 50% of probability of carrying the electron. In other words, a measurement localizes the electron in one of the two protons with 50% of probability for each possibility. The probability density distribution coming from the interference between the vibrational and dissociative contributions displays from the beginning a complex structure for the nuclei and an almost negligible regular distribution for the electron. At this point we stress that what can be measured, that is, what it is an observable, is the total probability density and not the separate components. Nevertheless, this partitioning is useful, for example, to examine how large the effect of the dissociating part on the vibrating part by looking at the nuclear and electronic probability and flux densities is. In fact, notice that $\int_0^\infty \mathrm{d}r\, \rho(r,t) = \int_0^\infty \mathrm{d}r\, \rho_{\mathrm{vib}}(r,t) + \int_0^\infty \mathrm{d}r\, \rho_{\mathrm{dis}}(r,t)$ because $\int_0^\infty \mathrm{d}r\, \Delta\rho_{\mathrm{int}}(r,t) = 0$. Thus, $\Delta\rho_{\mathrm{int}}(r,t)$ represents the interaction between the vibrational and dissociative states; therefore, one should expect that $\lim_{t\to\infty}\Delta\rho_{\mathrm{int}}(r,t) = 0$ when the coherence between the two components disappears. Notice that $\Delta\rho_{\mathrm{int}}(r,t)$ decreases from 10 to 50 fs and again from 50 to 120 fs. In general, the probability density for the interference is localized between $r \approx 0.5a_0$ and $10a_0$, suggesting that beyond $r \approx 10a_0$ there is no vibrating H_2^+ but only dissociating $H + H^+$.

Figure 3 displays the flux densities for the electron and the nuclei. We analyze first the vibrational component. The nuclear flux density follows the same trend as its counterpart the nuclear probability density; that is, it is initially more or less regular (see plot at 10 fs) and then turns into a complex distribution with several reversals (wave packets traveling in opposite directions, bond stretch $j_{n,\mathrm{vib}}(r,t) > 0$, and bond compression $j_{n,\mathrm{vib}}(r,t) < 0$, as can be seen in the plots at 50 and 120 fs); however, the behavior of the electronic flux density is quite different. For example, at 10 fs we observe a negative electronic flux density, even where the nuclear flux density is positive (beyond $r \approx 2a_0$). At 50 and 120 fs the electronic flux density is negligible compared with the nuclear flux density. This is a consequence of the dispersion of the nuclear probability density because on average the electron is subject to a pseudostationary nuclear distribution, leading to the vanishing electronic flux density.

The dissociative contributions to the flux densities appear rather simple. The electronic flux density resembles a Gaussian distribution centered on the nuclear flux density at all times, corresponding to two protons traveling in opposite directions, as expected from the probability density. (Compare the second row of Figure 2 with the second row of Figure 3.) The interfering components of the flux densities are also quite similar to the interfering components of the probability densities, in that we find a complex structure in the nuclear flux density and a negligible electronic flux density.

Now we proceed to discuss the nuclear probability density and the nuclear flux density in more detail. Figure 4 displays (a) the flux densities, (b) the probability densities, and (c) two bound states $\xi_{18}(R = 2r)$ and $\xi_{19}(R = 2r)$ and a continuum state $\xi_{149}(R = 2r)$ embedded in the potential energy curve $V(R = 2r)$ for $t = 120$ fs. Notice the long oscillating tail of $\Delta\rho_{n,\mathrm{int}}(r,t)$ and $\Delta j_{n,\mathrm{int}}(r,t)$. This can be understood by considering the two highest bound states $\nu = 18$ and 19 and a representative continuum state, for example, $\nu = 149$. (See Figure 4c.) Clearly

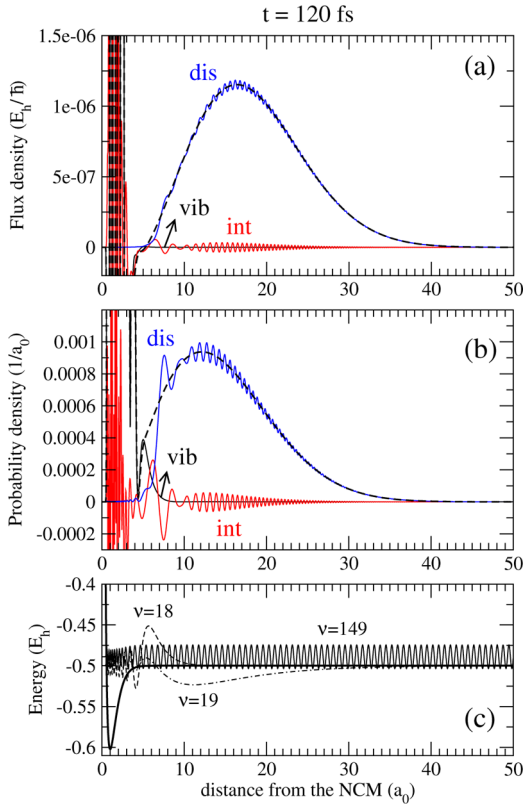

Figure 4. (a) Nuclear flux densities. (b) Nuclear probability densities. The total (vibrating, dissociating, and interfering) nuclear flux and probability densities are show with black dashed lines. The vibrating, dissociating, and interfering parts are shown with black, blue, and red solid lines, respectively. (c) Bound states $\xi_{18}(R = 2r)$ and $\xi_{19}(R = 2r)$ and continuum state $\xi_{149}(R = 2r)$ (with energy E_{149}=−0.4892E_h) embedded in the potential energy curve $V(R = 2r)$. The time propagation is $t = 120$ fs.

those eigenstates overlap, contributing to the long tail of the interfering components of the probability density and flux density. The interference is more pronounced in the probability density than in the flux density. At this point we discuss a limitation of this method, that is, the procedure of partitioning the total wave function into vibrational and dissociative components. As previously mentioned, the interfering component should vanish for $t \to \infty$. Judging from Figure 4c, one would be tempted to test this conclusion by propagating the wave function for a longer time, so that the dissociative contribution is distributed beyond $r = 50a_0$ (where the bound states go to zero), and the interfering components vanish. Such propagation would require a larger box for the *B*-spline basis functions to account for appropriate discretization of the continuum states. (One should avoid unphysical reflection of the nuclear wave packet.) However, the larger box would give rise to new bound states (presumably halo-states[17]), which would again be delocalized over the box. Thus, the vanishing of the interfering components of the densities cannot be realized in the practice. However, one can compromise by propagating the wave function until the interfering components decrease below a

DOI: 10.1021/acs.jpca.5b00907
J. Phys. Chem. A 2015, 119, 2895−2901

prescribed threshold. The present calculations suggest that the flux density separates more definitively into the vibrational and dissociative components when compared with the probability density. In other words, the coherences are less manifest in the flux densities than in the probability densities. (Consider the effect of $\Delta j_{n,\mathrm{int}}(r,t)$ on the total flux and the effect of $\Delta\rho_{n,\mathrm{int}}(r,t)$ on the total probability density.)

Finally, we examine the electronic probability density and the electronic flux density. (See Figure 5.) It is noteworthy that

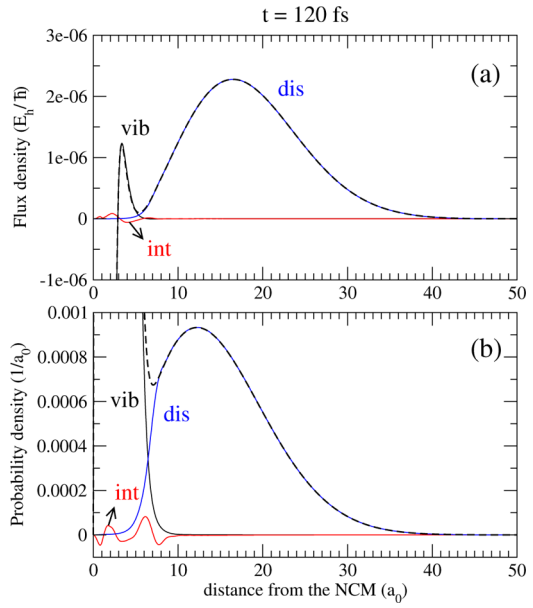

Figure 5. (a) Electronic flux densities. (b) Electronic probability densities. The total (vibrating, dissociating, and interfering) electronic flux and probability densities are shown with black dashed lines. The vibrating, dissociating, and interfering parts are shown with black, blue, and red solid lines, respectively. The time propagation is t = 120 fs.

both interfering components vanish for distances larger than $10a_0$. This observation can be explained in the same way as before for the vibrating part for long time propagations (50 and 120 fs); that is, the oscillating tail of the nuclear interfering probability density and flux density is experienced on average by the electron as a pseudostationary nuclear distribution. The interfering components of the electronic distribution are appreciable only at small distances. Thus, one can take the vibrational and dissociative components as the "true" electronic fluxes for the vibrating and dissociating H_2^+, respectively, because the interfering part is already negligible at t = 120 fs.

4. SUMMARY AND CONCLUSIONS

We have extended the theory for calculating the concerted nuclear and electronic probability densities and flux densities of the isotropic vibrating and dissociating H_2^+ ion. Previously the theory had been developed only for the vibration.[14] The formalism is based on the expansion of the radial nuclear wave function in terms of the vibrational eigenstates and the discretized continuum states. This framework yields nuclear and electronic probability densities and flux densities ($\rho_{n,\mathrm{vib}}$, $\rho_{e,\mathrm{vib}}$, $\mathbf{j}_{n,\mathrm{vib}}$, and $\mathbf{j}_{e,\mathrm{vib}}$, respectively) for the isotropic vibrating H_2^+ (pulsating quantum bubble) as well as nuclear and electronic probability densities and flux densities ($\rho_{n,\mathrm{dis}}$, $\rho_{e,\mathrm{dis}}$, $\mathbf{j}_{n,\mathrm{dis}}$, and $\mathbf{j}_{e,\mathrm{vib}}$, respectively) for the isotropic dissociating H_2^+ (exploding quantum bubble). The method also accounts for coherences between the isotropic vibrating and dissociating H_2^+, that is, interferences between the pulsating and the exploding quantum bubbles named $\Delta\rho_{n,\mathrm{int}}$, $\Delta\rho_{e,\mathrm{int}}$, $\Delta\mathbf{j}_{n,\mathrm{int}}$, and $\Delta\mathbf{j}_{e,\mathrm{int}}$. Such interferences disappear at long times. We find that such coherences vanish faster in the nuclear flux density than in the nuclear probability density, while they become almost imperceptible in both the electronic flux density and the electronic probability density. To the best of our knowledge, no such analysis has ever been reported in the literature, where we found calculation of flux densities either for vibrating systems[8,9,11−13] or for colliding (dissociating) systems[8] but not for scenarios when vibration and dissociation take place at the same time. We also notice that for the specific case considered here the dissociating part of the nuclear wave packet has a small effect on the nuclear flux density of the vibrating part, validating the conjectures observed in the nuclear flux density deduced from the experimental nuclear probability density data for the D_2^+ molecular ion.[6] These findings suggest that, in general, during molecular photoionization processes the flux density, for instance, the nuclear flux density $\mathbf{j}_n(\mathbf{R},t)$, is more suitable for separating the vibrational and dissociative components. This observation agrees well with the "virtual detector" method,[21] which makes use of the flux density as a suitable quantity to extract momentum distributions from wave-packet simulations.

AUTHOR INFORMATION

Corresponding Author

*Phone: +49 (0) 30 838 53348. Fax: +49 (0) 30 838 54792. E-mail: jperez@zedat.fu-berlin.de.

Notes

The authors declare no competing financial interest.

ACKNOWLEDGMENTS

The author expresses his gratitude to Professor D. J. Diestler (Lincoln), Professor J. Manz (Berlin), and Professor B. Paulus (Berlin) for their continuous support. The Computing Services Unit of the Zentraleinrichtung für Datenverarbeitung (ZEDAT) at Freie Universität Berlin is gratefully acknowledged for allocation of computer time. This work was supported by Deutsche Forschungsgemeinschaft under grant no. PE 2297/1-1.

REFERENCES

(1) Schrödinger, E. Quantisierung als Eigenwertproblem (Vierte Mitteilung). *Ann. Phys. (Leipzig)* **1926**, *81*, 109−139.

(2) Frohnmeyer, T.; Baumert, T. Femtosecond pump-probe photoelectron spectroscopy on Na_2: A tool to study basic coherent control schemes. *Appl. Phys. B: Laser Opt.* **2000**, *71*, 259−266.

(3) Ergler, T.; Rudenko, A.; Feuerstein, B.; Zrost, K.; Schröter, C. D.; Moshammer, R.; Ullrich, J. Spatiotemporal imaging of ultrafast molecular motion: Collapse and revival of the D_2^+ nuclear wave packet. *Phys. Rev. Lett.* **2006**, *97*, 193001.

(4) Eberly, J. H.; Narozhny, N. B.; Sanchez-Mondragon, J. J. Periodic Spontaneous Collapse and Revival in a Simple Quantum Model. *Phys. Rev. Lett.* **1980**, *44*, 1323−1326.

(5) Averbukh, I. S.; Vrakking, M. J. J.; Villeneuve, D. M.; Stolow, A. Wave packet isotope separation. *Phys. Rev. Lett.* **1996**, *77*, 3518.

(6) Manz, J.; Pérez-Torres, J. F.; Yang, Y. Nuclear Flux Densities in Diatomic Molecules Deduced from High-Resolution Pump-Probe Spectra with Spatiotemporal Resolutions down to 5 pm and 200 asec. *Phys. Rev. Lett.* **2013**, *111*, 153004.

(7) Lafosse, A.; Lebech, M.; Brenot, J. C.; Guyon, P. M.; Spielberger, L.; Jagutzki, O.; Houver, J. C.; Dowek, D. Molecular frame photoelectron angular distributions in dissociative photoionization of

DOI: 10.1021/acs.jpca.5b00907
J. Phys. Chem. A 2015, 119, 2895−2901

H_2 in the region of the Q_1 and Q_2 doubly excited states. *J. Phys. B: At. Mol. Opt. Phys.* **2003**, *36*, 4683.
(8) Okuyama, M.; Takatsuka, K. Electron flux in molecules induced by nuclear motion. *Chem. Phys. Lett.* **2009**, *476*, 109−115.
(9) Barth, I.; Hege, H.-C.; Ikeda, H.; Kenfack, A.; Koppitz, M.; Manz, J.; Marquardt, F.; Paramonov, G. K. Concerted Quantum Effects of Electronic and Nuclear Fluxes in Molecules. *Chem. Phys. Lett.* **2009**, *481*, 118−123.
(10) Diestler, D. J. Coupled-channels Quantum Theory of Electronic Flux Density in Electronically Adiabatic Processes: Fundamentals. *J. Phys. Chem. A* **2012**, *116*, 2728−2735.
(11) Diestler, D. J.; Kenfack, A.; Manz, J.; Paulus, B. Coupled-Channels Quantum Theory of Electronic Flux Density in Electronically Adiabatic Processes: Application to the Hydrogen Molecule Ion. *J. Phys. Chem. A* **2012**, *116*, 2736−2742.
(12) Diestler, D. J.; Kenfack, A.; Manz, J.; Paulus, B.; Pérez-Torres, J. F.; Pohl, V. Computation of the Electronic Flux Density in the Born-Oppenheimer Approximation. *J. Phys. Chem. A* **2013**, *117*, 8519−8527.
(13) Pérez-Torres, J. F. Electronic Flux Densities in Vibrating H_2^+. in Terms of Vibronic Eigenstates. *Phys. Rev. A* **2013**, *87*, 062512:1−7.
(14) Manz, J.; Pérez-Torres, J. F.; Yang, Y. Vibrating $H_2^+(^2\Sigma_g^+,JM = 00)$ Ion as a Pulsating Quantum Bubble in the Laboratory Frame. *J. Phys. Chem. A* **2014**, *118*, 8411−8425.
(15) Martin, F. Ionization and dissociation using B-splines: photoionization of the hydrogen molecule. *J. Phys. B: At. Mol. Opt. Phys.* **1999**, *32*, R197.
(16) Bachau, H.; Cormier, E.; Decleva, P.; Hansen, J. E.; Martín, F. Applications of B-splines in atomic and molecular physics. *Rev. Prog. Phys.* **2001**, *64*, 1815−1942.
(17) Derevianko, A.; Luc-Koenig, E.; Masnou-Seeuws, F. Application of B-splines in determining the eigenspectrum of diatomic molecules: robust numerical description of halo-state and Feshbach molecules. *Can. J. Phys.* **2009**, *87*, 67−74.
(18) Åsbrink, L. The Photoelectron Spectrum of H_2. *Chem. Phys. Lett.* **1970**, *7*, 549−552.
(19) Werner, H.-J., Knowles, P. J., Knizia, G., Manby, F. R., Schütz, M., Celani, P., Korona, T., Lindh, R., Mitrushenkov, A., Rauhut, G. et al. MOLPRO, version 2012.1, a package of ab initio programs 2012.
(20) Hermann, G., Pohl, V., Schild, A. A Toolbox for Post-Processing Quantum Chemical Wavefunction Data, 2014. http://sourceforge.net/p/orbkit/.
(21) Feuerstein, B.; Thumm, U. On the computation of momentum distributions within wavepacket propagation calculations. *J. Phys. B: At. Mol. Opt. Phys.* **2003**, *36*, 707−716.

DOI: 10.1021/acs.jpca.5b00907
J. Phys. Chem. A 2015, 119, 2895−2901